Nanoscale

PAPER

View Article Online
View Journal | View Issue

Open Access Article. Published on 13 February 2018. Downloaded on 12/4/2025 9:16:04 PM.
This article is licensed under a Creative Commons Attribution-NonCommercial 3.0 Unported Licence.

Check for updates

Cite this: *Nanoscale*, 2018, **10**, 4123

Compartmentalized supramolecular hydrogels based on viral nanocages towards sophisticated cargo administration†

Liulin Yang,[a,b] Aijie Liu,[a] Mark V. de Ruiter,[a] Catharina. A. Hommersom,[a] Nathalie Katsonis,[a] Pascal Jonkheijm *[b] and Jeroen J. L. M. Cornelissen *[a]

Introduction of compartments with defined spaces inside a hydrogel network brings unique features, such as cargo quantification, stabilization and diminishment of burst release, which are all desired for biomedical applications. As a proof of concept, guest-modified cowpea chlorotic mottle virus (CCMV) particles and complementary guest-modified hydroxylpropyl cellulose (HPC) were non-covalently cross-linked through the formation of ternary host–guest complexes with cucurbit[8]uril (CB[8]). Furthermore, CCMV based virus-like particles (VLPs) loaded with tetrasulfonated zinc phthalocyanine (ZnPc) were prepared, with a loading efficiency up to 99%, which are subsequently successfully integrated inside the supramolecular hydrogel network. It was shown that compartments provided by protein cages not only help to quantify the loaded ZnPc cargo, but also improve the water solubility of ZnPc to avoid undesired aggregation. Moreover, the VLPs together with ZnPc cargo can be released in a controlled way without an initial burst release. The photodynamic effect of ZnPc molecules was retained after encapsulation of capsid protein and release from the hydrogel. This line of research suggests a new approach for sophisticated drug administration in supramolecular hydrogels.

Received 16th October 2017,
Accepted 3rd December 2017

DOI: 10.1039/c7nr07718a

rsc.li/nanoscale

Introduction

Supramolecular hydrogels[1–4] are a class of 3D cross-linked materials driven by non-covalent interactions, including hydrophobic interactions,[5,6] multiple hydrogen bonding interactions,[7–9] metal-coordination,[10–12] electrostatic interactions,[13–16] and host–guest interactions.[17–20] The dynamic non-covalent bonds endow supramolecular hydrogels with unique properties, such as reversibility, self-healing, stimuli responsiveness. Therefore, supramolecular hydrogels have been of great interest for a wide range of biomedical applications such as bio-sensing, controlled drug release and tissue engineering.[2,3] Besides these advantages, a sophisticated cargo administration of supramolecular hydrogel, such as cargo quantification, stabilization and diminishment of initial burst release, remains challenge. Initial burst release of cargo molecules from supramolecular hydrogels could be serious due to weak interactions between the cargo and hydrogel matrix and, is generally undesirable for controlled drug release.[21,22]

To address this challenge, we report supramolecular hydrogels with defined compartments by employing viral nanocages towards sophisticated cargo quantification, stabilization and sustained release. Virus nanoparticles and the derived virus-like particles (VLPs), are well-known for their reversible assembly–disassembly, monodisperse particle size, and capability of cargo encapsulation.[23–26] They have been widely studied for broad applications such as catalysis, scaffolds in hydrogel for tissue engineering.[27–32] Compartments created by viral nanocages within hydrogels may bring several unique features. First, viral nanocages are excellent nanocontainers to encapsulate various cargos, the forming particles are generally robust under broad pH, salt and temperature ranges.[33] Labile cargos can thus be protected by protein cages. Second, the defined compartment in virus particles could facilitate the quantification of drugs, which is crucial for drug administration. In that way, the initial burst release could be inhibited due to the immobilization of VLPs. Third, the exterior surface of viral nanocages are easily to be functionalized,[34] which helps them to be involved in the formation of hydrogel network.

As a proof of concept, we tried to build supramolecular hydrogels with homogeneous compartments by incorporating cowpea chlorotic mottle virus (CCMV) as well as the derived VLPs through host–guest interaction. CCMV is an icosahedral

[a]*Laboratory for Biomolecular Nanotechnology, MESA+ Institute for Nanotechnology, University of Twente, P.O. Box 217, 7500 AE Enschede, The Netherlands. E-mail: J.J.L.M.Cornelissen@utwente.nl*
[b]*Molecular Nanofabrication Group, MESA+ Institute for Nanotechnology, University of Twente, P.O. Box 217, 7500 AE Enschede, The Netherlands. E-mail: P.Jonkheijm@utwente.nl*

†Electronic supplementary information (ESI) available. See DOI: 10.1039/c7nr07718a

Open Access Article. Published on 13 February 2018. Downloaded on 12/4/2025 9:16:04 PM.
This article is licensed under a Creative Commons Attribution-NonCommercial 3.0 Unported Licence.

plant virus with inner and outer diameters of 18 and 28 nm, respectively.[35] CCMV capsid disassembles into 90 identical coat protein dimers (CPs) at neutral pH and high ionic strength. After removal of viral RNA, the CPs can re-assemble into VLPs with different sizes and shapes under different conditions of pH, ionic strength and with different cargos.[36–38] Encapsulation of a variety of these cargos, including DNA,[39,40] enzymes,[41] negatively charged polymers[42] and organic molecules,[43,44] gold nanoparticles,[45,46] quantum dots[47] and magnetic nanoparticles,[48] has resulted in the formation of functionalized VLPs. Therefore, CCMV based protein cages are good candidates as nanocontainers to build compartmentalized supramolecular hydrogels.

To this end, CCMV nanoparticles were non-covalently cross-linked with hydroxylpropyl cellulose (HPC) by a ternary host–guest interaction, including cucurbit[8]uril (CB[8]) as a host and methyl viologen and naphthyl as guests. Two pathways have been studied to prepare the supramolecular hydrogels (Scheme 1). In pathway A, CCMV is modified with methyl viologen groups (CCMV-Vio) and HPC with naphthyl groups (HPC-Np); pathway B aims to modify CCMV with naphthyl groups (CCMV-Np) and HPC with methyl viologen groups (HPC-Vio). The investigation of the preparation pathway in the formation of a supramolecular hydrogel is rare. It is, however, of guiding significance in the design of compartmentalized supramolecular hydrogels. Based on this study, CCMV based VLPs with tetrasulfonated zinc phthalocyanine (ZnPc) as cargo were used to prepare functionalized supramolecular hydrogels with loaded compartments. Cargo release was studied and compared to the conventional supramolecular hydrogel without protein cages. Photodynamic effects of free ZnPc, VLPs (CCMV/ZnPc) and released VLPs were investigated *in vitro*.

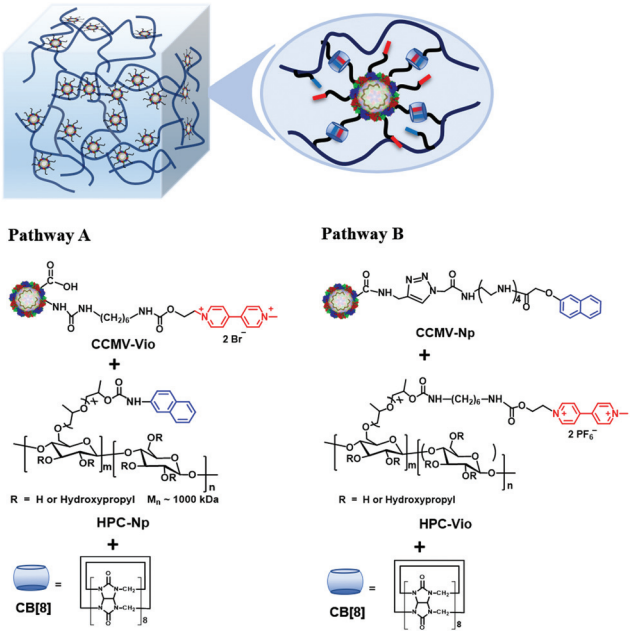

Scheme 1 Two pathways to prepare compartmentalized supramolecular hydrogels based on virus nanoparticles. Polymeric material HPC and CCMV nanoparticles were cross-linked through a ternary host–guest interaction, which involved methyl viologen and naphthyl moieties and CB[8].

Results and discussion

Successful preparation of CCMV-Vio was confirmed by adding sodium dithionite, which reduced the methyl viologen into a single charged state with a characteristic absorption around λ = 550 nm in UV-Vis spectrum, as shown in Fig. 1a. Meanwhile, the color of the solution turned deep purple (Fig. 1a, inset), which is characteristic for single charged viologen. The average number of methyl viologen groups per capsid protein per capsid protein unit was estimated to be ~2.1 (ESI, section 3.1†). In other words, each CCMV nanoparticle contained ~378 methyl viologen groups, giving sufficient handles for supramolecular cross-linking. Inspection by TEM microscopy (Fig. 1b) showed that the virus particles maintained a spherical shape after conjugation, and that the size of particles was consistent with the size observed using DLS (ESI, Fig. S1†). Successful modification of CCMV with the Np group was confirmed by the appearance of a shoulder at λ = 325 nm in UV-Vis spectrum (Fig. 1c). The content of the Np group was estimated to be around 1.0 per capsid protein, *i.e.* about 180 Np groups on each protein cage. TEM (Fig. 1d) and DLS (ESI Fig. S3†) analysis showed a narrow distribution of CCMV-Np particles, the average size was about 18 nm, which was smaller than native CCMV. The reason for such a contraction is not clear yet, however, the conjugation of hydrophobic Np groups on the particle surface could play a role in this.

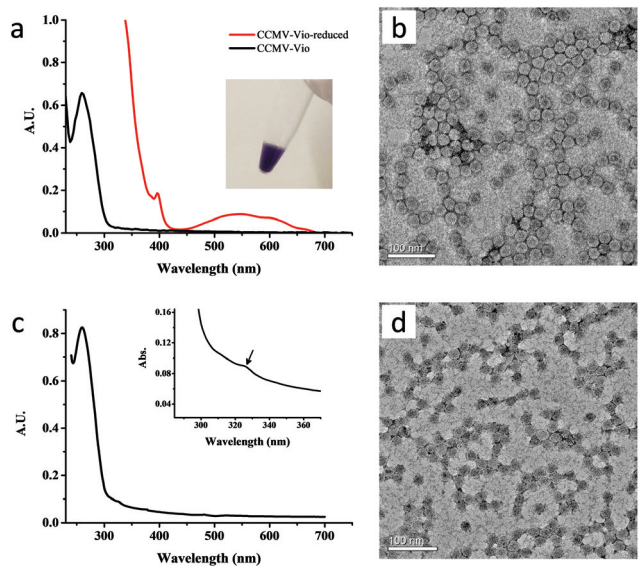

Fig. 1 (a) UV-Vis spectra of CCMV-Vio before (black curve) and after reduction (red curve). Inset: solution of reduced CCMV-Vio. (b) Negatively stained TEM image of CCMV-Vio. (c) UV-Vis spectra of CCMV-Np. (d) Negatively stainned TEM images of CCMV-Np showed spherical and monodispersed nanoparticles with size around 18 nm.

 This journal is © The Royal Society of Chemistry 2018

Open Access Article. Published on 13 February 2018. Downloaded on 12/4/2025 9:16:04 PM.
This article is licensed under a Creative Commons Attribution-NonCommercial 3.0 Unported Licence.

HPC, with a number-average molecular weight of 1000 kDa, was selected as a polymeric material for the hydrogel. The content of naphthalene groups in HPC-Np was estimated to be 75 μmol per gram of polymer. The degree of substitution should not be too high, otherwise, the water solubility of HPC-Np will dramatically decrease due to the hydrophobicity of the naphthyl groups. For HPC-Vio, the content of methyl viologen group was 68 μmol per gram of polymer.

With these materials in hand, we prepared the supramolecular hydrogel in two different ways. In pathway A, CCMV-Vio, HPC-Np and CB[8] were mixed while the ratio of methyl viologen group, naphthyl group and CB[8] was 1 : 1 : 1. In pathway B, CCMV-Np, HPC-Vio and CB[8] were mixed also with an equal molar ratio of methyl viologen, naphtyl and CB[8]. The formation of a hydrogel can be simply judged from apparent fluidity of the material. The 4 wt% of HPC-Np is a sticky fluid, in contrast, the supramolecular hydrogel formed from pathway A with 4 wt% of HPC-Np is a self-standing, jelly like material (ESI Fig. S5a†). The host–guest interaction among these three components was evidenced by absorption around 400–500 nm in UV-Vis spectrum (ESI Fig. S5c†), which is ascribed to the charge transfer interaction between the naphthyl and methyl viologen groups inside the cavity of CB[8].[49] To verify that the gelation was caused by supramolecular crosslinking, HPC-Np, CCMV-Vio, and CB[7] were mixed as a control experiment. In this case, no hydrogel formed, only a turbid solution without a color change (ESI, Fig. S5b†). CB[7] can only encapsulates one guest molecule inside the cavity, therefore, polymer chains and virus nanoparticles cannot be crosslinked by CB[7].

The structure of the formed hydrogels was investigated by scanning electron microscopy (SEM). Network structures were observed at low magnification for hydrogels from both pathways (Fig. 2a & c). At high magnification, well-defined nanoparticles with a diameter around 20–30 nanometer dispersed in the polymer matrix were found, in line with the presence of viral nanoparticles (Fig. 2b & d), indicating successful integration in the hydrogels.

Rheology studies were performed to further confirm the formation of supramolecular hydrogels. The storage and loss modulus of the hydrogels are in a typical range for similar materials.[19] For the hydrogel from pathway A, when the content of the polymer was 4 wt%, the storage modulus was slightly higher than the loss modulus, and the values of these two moduli were relatively low (around 100 Pa) (Fig. 2e). However, when the content of polymer was raised to 6 wt%, both of the two moduli increased significantly (around 300 Pa), and the storage modulus was significantly higher than the loss modulus, indicating viscoelastic properties of the hydrogel. For the hydrogel from pathway B, when the content of HPC-Vio was only 1 wt%, the storage modulus was already higher than loss modulus, although the values of the two moduli were relatively low (Fig. 2g). The difference of the two moduli was more significant for the 2 wt% sample, both of them were higher than the 1 wt% sample, and were comparable to the 4 wt% hydrogel prepared through pathway A. It should be noted that the gel point (cross point of two moduli)

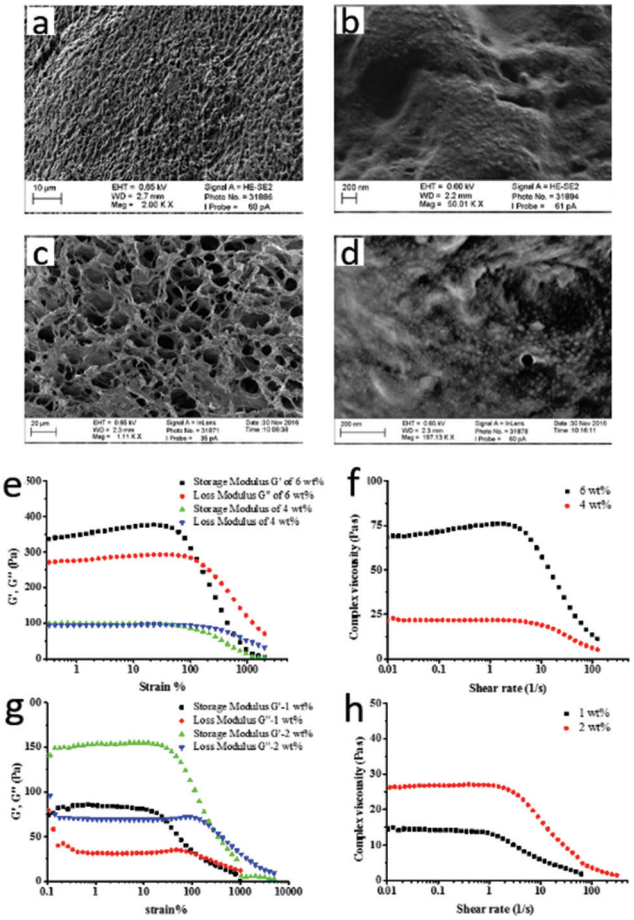

Fig. 2 (a) SEM images of 4 wt% supramolecular hydrogel formed through pathway A. A network structure obtained after lyophilization of supramolecular hydrogel. The scale bar is 10 μm. (b) CCMV-Vio particles dispersed in the polymer matrix of 4 wt% hydrogel. The scale bar is 200 nm. (c) SEM images of 2 wt% supramolecular hydrogel formed through pathway B. A highly porous network obtained after lyophilization of supramolecular hydrogel. The scale bar is 20 μm. (d) Virus nanoparticles dispersed in the polymer matrix of 2 wt% hydrogel. The scale bar is 200 nm. (e), (f) Rheology study of supramolecular hydrogel formed by pathway A. (g), (h) Rheology study of supramolecular hydrogel formed by pathway B.

in the 2 wt% sample was around 250%, which was much higher than 4 wt% hydrogel from pathway A. That means the supramolecular hydrogel prepared in pathway B has improved mechanical properties compared to that of pathway A. The reason could be that the positively charged HPC-Vio is a polyelectrolyte with a higher viscosity in solution compared to the uncharged HPC polymer, which improves the mechanical strength of supramolecular hydrogel. Both of modulus (Fig. 2e & g) and viscosity (Fig. 2f & h) of the hydrogels decreased quickly when the strain or shear rate increased to a certain value, which means that the network of hydrogel was destroyed, and the hydrogel turned to be more fluidic. This shear-thinning property is characteristic to the formation of supramolecular hydrogels, which makes them promising to be used for example as an injectable material for biomedical applications.

Open Access Article. Published on 13 February 2018. Downloaded on 12/4/2025 9:16:04 PM.
This article is licensed under a Creative Commons Attribution-NonCommercial 3.0 Unported Licence.

The hydrogel preparation following pathway A, which involves CCMV-Vio and HPC-Np, is relatively easy. CCMV particles conjugated with methyl viologen groups are stable and monodisperse. However, it needs a relatively high concentration of HPC-Np (at least 4 wt%) to ensure the formation of a hydrogel with sufficient mechanical strength. In pathway B, which involves CCMV-Np and HPC-Vio, a lower concentration of polymeric material (2 wt%) is needed to obtain a self-standing hydrogel, even though the CCMV particles are less conjugated. The apparent viscosity of polyelectrolyte HPC-Vio solutions is higher than that of HPC-Np, which facilitates the formation of hydrogel. However, the preparation of CCMV-Np involves a tedious organic synthesis, including a copper catalyzed click reaction on CCMV particles. Performing the click reaction under dilute concentrations (*e.g.* 1 mg mL^{-1}) in an inert atmosphere and specifically designed reagents, such as tris(3-hydroxypropyltriazolylmethyl)amine and aminoguanidine, are necessary to avoid side-reactions that cause crosslinking and aggregation of virus particles.[50] Given these reasons, pathway A was selected to prepare a functionalized supramolecular hydrogel for studies with cargo loaded virus-like particles.

Phthalocyanines (Pc) are promising materials for photodynamic therapy.[51–53] However, on account of a poor water solubility, they highly tend to aggregate in buffer solution, which hampers the application.[52] Encapsulation of Pc into VLPs not only improves the solubility of Pc, but also helps to improve the biocompatibility of Pc, which is very appealing for biomedical applications.[43] Therefore, tetrasulfonated zinc phthalocyanine (ZnPc) was encapsulated in the CCMV capsid yielding virus-like particles (CCMV/ZnPc), and these nanoparticles were then integrated into the supramolecular hydrogel network to prepare a functional supramolecular hydrogel.

Preparation of CCMV/ZnPc was performed according to a literature procedure (details in ESI, section 3.6†).[43] On account of the electrostatic interaction between negatively charged ZnPc and positive charged N-terminals of capsid proteins, the encapsulation efficiency of ZnPc was nearly quantitative (~99%), based on the integration of FPLC peaks. Based on the optical data, the number of ZnPc was estimated to be 180 in each protein cage, which is close to the reported data.[37] It should be noted that after encapsulation, the bulk concentration of ZnPc could be increased to mM level in buffer solution without further aggregation for months, while free ZnPc tend to aggregate and precipitate in hours (ESI, Fig. S8†). The compartments provided by protein cages help to disperse and stabilize the ZnPc molecules in solution.

CCMV/ZnPc particles were then conjugated with methyl viologen groups to prepare CCMV-Vio/ZnPc particles (Fig. 3a). The detailed procedure is given in the ESI (ESI section 3.7†). The CCMV-Vio/ZnPc particles were characterized using UV-Vis spectroscopy. As shown in Fig. 3b, the methyl viologen group has a single absorption peak at λ = 260 nm, which partially overlaps with the absorption of the capsid protein at λ = 280 nm. Therefore, the conjugation of methyl viologen groups on CCMV/ZnPc is confirmed by an increase of the I_{260}/I_{280} ratio in the UV-Vis spectrum from 0.57 to 0.94 after modification. The absorption intensity of ZnPc decreased after reaction, and the number of ZnPc in each protein cage was estimated to be 113, suggesting a partially loss of ZnPc cargo molecules during the surface modification. This may be due to an electrostatic interaction between positively charged methyl viologen groups and negatively charged ZnPc molecules, which results in leakage of ZnPc molecules from the protein cages. Unfortunately, the quantification of the number of methyl viologen groups was difficult using the same method as before (see above), because the interference of cargo ZnPc. Therefore, the number of attached methyl viologen groups was estimated by subtracting the absorption of capsid proteins and ZnPc from the UV-Vis spectrum of CCMV-Vio/ZnPc. The number of methyl viologen group was estimated in this way to be 1.5 per capsid protein, which is comparable to the CCMV-Vio particles. The nanoparticles remained dispersed after modification, no significant aggregation was observed, according to the results of TEM and DLS analysis (Fig. 3c & d). DLS data showed that the average size of CCMV-Vio/ZnPc particles was around 14–18 nm, which is consistent with TEM observations and the previously determined T = 1 structure.[44]

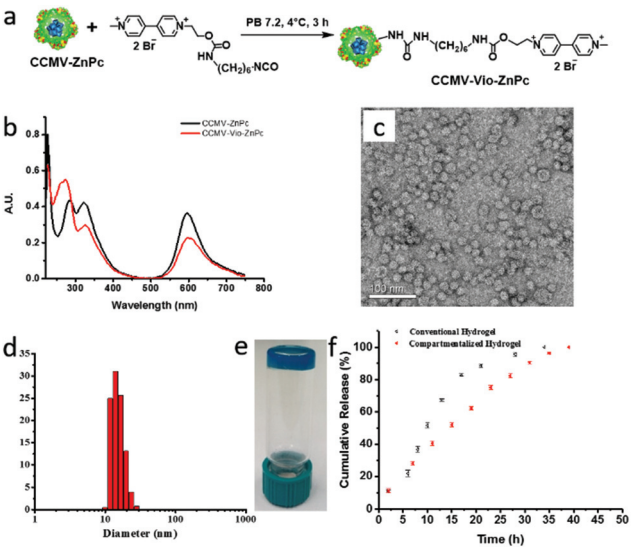

Fig. 3 (a) Conjugation route of CCMV-Vio/ZnPc. (b) UV-Vis spectra of CCMV/ZnPc and CCMV-Vio/ZnPc. (c) TEM image of CCMV-Vio/ZnPc. (d) Particle size of CCMV-Vio/ZnPc measured by DLS. (e) 4 wt% supramolecular hydrogel with deep blue color formed by CCMV-Vio/ZnPc, HPC-Np and CB[8]. (f) Cargo release profiles of compartmentalized and conventional supramolecular hydrogels.

Functionalized supramolecular hydrogels were prepared by CCMV-Vio/ZnPc, CB[8] and HPC-Np in the same way as mentioned above. In a typical experiment, a supramolecular hydrogel with 4 wt% of HPC polymer showed a deep blue color, indicating that the ZnPc was successfully integrated inside the hydrogel (Fig. 3e). As comparison, a conventional supramolecular hydrogel with 4 wt% of polymer was constructed by non-covalent crosslinking of HPC-Np, HPC-Vio, and CB[8], with ZnPc simply mixed into hydrogel network (details in ESI,

Open Access Article. Published on 13 February 2018. Downloaded on 12/4/2025 9:16:04 PM.
This article is licensed under a Creative Commons Attribution-NonCommercial 3.0 Unported Licence.

section 2.7†). Rheology experiments revealed a weaker mechanical performance of the conventional hydrogel (moduli of 10^1 Pa) compared to compartmentalized hydrogel (moduli of 10^2 Pa) (details in ESI, section 3.8†).

The release profiles, as monitoring by the UV-Vis absorption of the ZnPc showed a smooth and nearly linear release of cargo from the compartmentalized supramolecular hydrogel (Fig. 3f). In contrast, an initial faster release of ZnPc was observed for the conventional supramolecular hydrogel, similar to the other supramolecular systems.[5,17] The initial fast release of ZnPc for the conventional hydrogel should be ascribed to the simple physical absorption of cargo in the network, and the relatively weak mechanical performance. The results suggests a better administration of cargo by compartmentalized hydrogels.

To study the release mechanism of the compartmentalized supramolecular hydrogel, the released solutions were concentrated and analyzed by FPLC and TEM. In the FPLC chromatogram, a main peak with elution volume corresponding to the void volume of column was observed (details in ESI, section 3.9†), suggesting large particles in this solution. The strong absorption at λ = 600 nm of this fraction indicated the presence of ZnPc in these particles. TEM analysis of the collected fraction revealed that the large particles are VLPs aggregates covered by polymers. According to these results, we can conclude that it were the VLPs with encapsulated ZnPc cargo that released from the hydrogel. This process should be attributed to the erosion of hydrogel, *i.e.* a gradually disintegration of polymer network, due to the dynamic feature of host–guest interactions.[5] In this study, the VLPs are robust under the releasing conditions, therefore ZnPc can hardly escape from the protein cages, therefore, are released together with protein cages. This unique feature brings advantages in some cases: toxic or labile cargo molecules can still be protected by protein cages after release, which can decrease cytotoxicity or prolong half-life-time of drug cargos. Moreover, the versatile character of the protein cage surface facilitates its modification in order to improve biocompatibility and efficiency of targeted drug delivery.

The photodynamic activity of released VLPs were investigated in cell experiments. In parallel experiments, free ZnPc, VLPs (CCMV/ZnPc) and the released VLPs from hydrogel were incorporated by RAW 264.7 macrophage cells (obtained from The American Type Culture Collection), and followed by irradiation for 60 min using a halogen lamp (with a high-pass filter > 500 nm, 15 mW cm^{-2} at λ = 600 nm) (details in ESI, section 2.9†). The cells were stained with a DNA intercalating stain, propidium iodide (PI). The PI stain indicates loss of plasma membrane integrity, as a consequence of *e.g.* cell death. As shown in Fig. 4, the dying and dead cells are identified as they appear red in the fluorescence images. In contrast to the cells without irradiation, all the three samples including ZnPc, VLPs and released VLPs can induce cell death upon cellular uptake and subsequent irradiation. A live/dead assay was performed and the results show that after irradiation, the viable cell in each set of samples decreased around 30–40%,

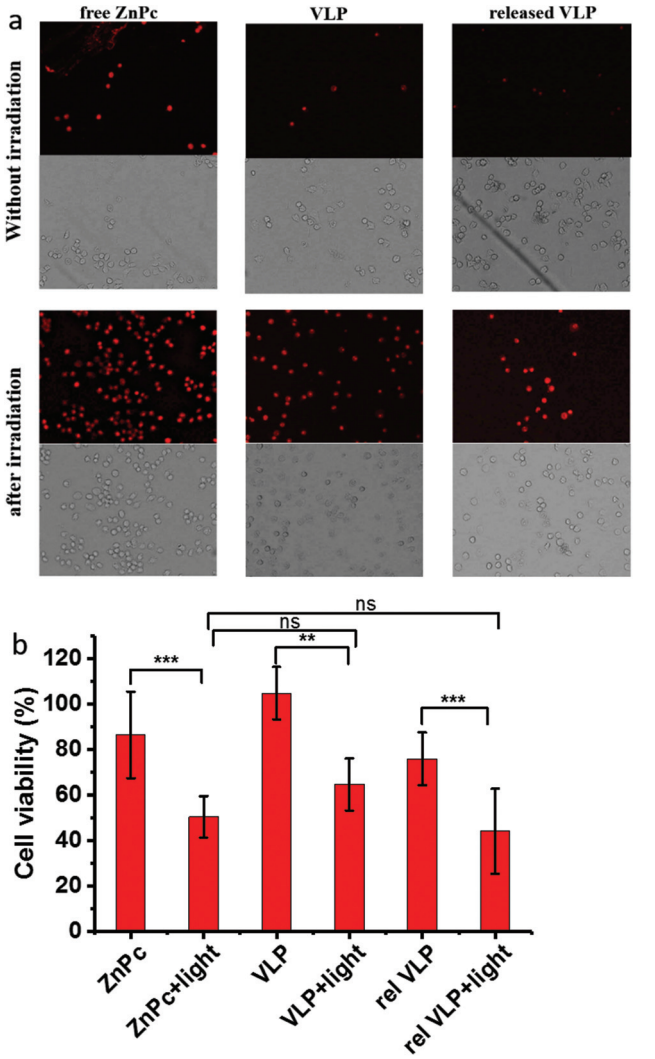

Fig. 4 (a) Optical images of RAW macrophage cells stained by propidium iodide (PI) in the presence of free ZnPc, VLPs and released VLPs without or after irradiation. (b) The viability of macrophage cells evaluated by a live/dead cell assay. Error bars represent the standard deviations corrected by error propagation. $^{**}p < 0.01$, $^{***}p < 0.001$, ns: no significance.

compared to the cells without irradiation. Based on the statistical analysis (ESI, section 3.10†), the difference of cell viability in each set of samples with/without irradiation has high statistical significance ($p < 0.01$), which further confirms the activity of ZnPc. The averaged reductions of cell viability for all the three sets of samples after irradiation were comparable (around 30–40%) with differences having relatively low practical significance. Meanwhile, analysis of variance (ESI, section 3.10†) also shows a low statistical significance ($p > 0.05$) for the differences between ZnPc/VLP and between ZnPc/rel VLP. All of these results suggest the retention of activity of ZnPc after encapsulation and releasing from the hydrogel. The photosensitizers including ZnPc are not efficient in killing cancer cells when used alone, due to the hypoxic nature of the cancer cell microenvironment. It has been shown that photo-

Open Access Article. Published on 13 February 2018. Downloaded on 12/4/2025 9:16:04 PM.
This article is licensed under a Creative Commons Attribution-NonCommercial 3.0 Unported Licence.

sensitizers coupled with peroxidase and glucose oxidase can effectively suppress the growth of tumour, by virtue of generation of $^1O_2$ *in situ*.[54] Protein cages are ideal nanocarriers to encapsulate multiple components. In future work, it is anticipated to improve the photodynamic therapy efficiency of VLPs by coupling photosensitizers with enzymes as combined medication.

Conclusions

In summary, compartmentalized supramolecular hydrogels have been constructed by integrating viral nanocages into hydrogel network. Different pathways to prepare supramolecular hydrogels through ternary host–guest interactions have been studied. Our present investigations eventually resulted in a supramolecular hydrogel containing functional CCMV/ZnPc VLPs with high cargo loading efficiency. The content of ZnPc in each protein cage can be estimated, the protein cages improve the water solubility of ZnPc, and the VLPs can be released in a controlled way without an initial burst release. These are all advantages over traditional dispersion of cargo molecules in a supramolecular hydrogel.

The introduction of these protein compartments inside hydrogel brings several new features, such as high loading efficiency, cargo quantification, stabilization and diminishment of burst release. Based on this strategy, different types of cargo[55,56] could be integrated in a hydrogel simultaneously, which is beneficial for combined medication. Loading can be easily controlled by, for example, tuning the ratio of VLPs that encapsulate different cargos. Furthermore, by introducing stimuli responsive VLPs, the compartmentalized hydrogel would be endowed with a high degree of manageability. Highly sophisticated drug administration can be envisioned, such as sequential drug release at definite time and quantity,[57] by controlling the release behavior of VLPs.

Conflicts of interest

There are no conflicts to declare.

Acknowledgements

We acknowledge the European Research Council for financial support by a Proof of Concept grant BioStealth (to PJ 641342) and a Consolidator grant ProtCage (to JJLMC 616907). We thank Robin Klem for the help of cell experiments, and Nicole Zeijen for the discussion of statistical analysis.

References

1 E. A. Appel, J. Del Barrio, X. J. Loh and O. A. Scherman, *Chem. Soc. Rev.*, 2012, **41**, 6195–6214.
2 R. Dong, Y. Pang, Y. Su and X. Zhu, *Biomater. Sci.*, 2015, **3**, 937–954.
3 X. Du, J. Zhou, J. Shi and B. Xu, *Chem. Rev.*, 2015, **115**, 13165–13307.
4 L. Voorhaar and R. Hoogenboom, *Chem. Soc. Rev.*, 2016, **45**, 4013–4031.
5 E. A. Appel, M. W. Tibbitt, M. J. Webber, B. A. Mattix, O. Veiseh and R. Langer, *Nat. Commun.*, 2015, **6**, 6295, DOI: 10.1038/ncomms7295.
6 K. Nagahama, D. Kawano, N. Oyama, A. Takemoto, T. Kumano and J. Kawakami, *Biomacromolecules*, 2015, **16**, 880–889.
7 P. Y. W. Dankers, T. M. Hermans, T. W. Baughman, Y. Kamikawa, R. E. Kieltyka, M. M. C. Bastings, H. M. Janssen, N. A. J. M. Sommerdijk, A. Larsen, M. J. A. van Luyn, A. W. Bosman, E. R. Popa, G. Fytas and E. W. Meijer, *Adv. Mater.*, 2012, **24**, 2703–2709.
8 J. Cui and A. D. Campo, *Chem. Commun.*, 2012, **48**, 9302–9304.
9 M. Guo, L. M. Pitet, H. M. Wyss, M. Vos, P. Y. W. Dankers and E. W. Meijer, *J. Am. Chem. Soc.*, 2014, **136**, 6969–6977.
10 Z. Sun, F. Lv, L. Cao, L. Liu, Y. Zhang and Z. Lu, *Angew. Chem., Int. Ed.*, 2015, **54**, 7944–7948.
11 D. E. Fullenkamp, L. He, D. G. Barrett, W. R. Burghardt and P. B. Messersmith, *Macromolecules*, 2013, **46**, 1167–1174.
12 J. Sun, X. Zhao, W. R. K. Illeperuma, O. Chaudhuri, K. H. Oh, D. J. Mooney, J. J. Vlassak and Z. Suo, *Nature*, 2012, **489**, 133–136.
13 T. L. Sun, T. Kurokawa, S. Kuroda, A. B. Ihsan, T. Akasaki, K. Sato, M. A. Haque, T. Nakajima and J. P. Gong, *Nat. Mater.*, 2013, **12**, 932–937.
14 F. Luo, T. L. Sun, T. Nakajima, T. Kurokawa, Y. Zhao, K. Sato, A. B. Ihsan, X. Li, H. Guo and J. P. Gong, *Adv. Mater.*, 2015, **27**, 2722–2727.
15 Q. Wang, J. L. Mynar, M. Yoshida, E. Lee, M. Lee, K. Okuro, K. Kinbara and T. Aida, *Nature*, 2010, **463**, 339–343.
16 J. N. Hunt, K. E. Feldman, N. A. Lynd, J. Deek, L. M. Campos, J. M. Spruell, B. M. Hernandez, E. J. Kramer and C. J. Hawker, *Adv. Mater.*, 2011, **23**, 2327–2331.
17 E. A. Appel, X. J. Loh, S. T. Jones, F. Biedermann, C. A. Dreiss and O. A. Scherman, *J. Am. Chem. Soc.*, 2012, **134**, 11767–11773.
18 E. Janeček, J. R. McKee, C. S. Y. Tan, A. Nykänen, M. Kettunen, J. Laine, O. Ikkala and O. A. Scherman, *Angew. Chem., Int. Ed.*, 2015, **54**, 5383–5388.
19 C. Li, M. J. Rowland, Y. Shao, T. Cao, C. Chen, H. Jia, X. Zhou, Z. Yang, O. A. Scherman and D. Liu, *Adv. Mater.*, 2015, **27**, 3298–3304.
20 E. A. Appel, F. Biedermann, U. Rauwald, S. T. Jones, J. M. Zayed and O. A. Scherman, *J. Am. Chem. Soc.*, 2010, **132**, 14251–14260.
21 L. Lin, M. Larsson and D. Liu, *Soft Matter*, 2011, **7**, 5816–5825.
22 M. Hsiao, M. Larsson, A. Larsson, H. Evenbratt, Y. Chen, Y. Chen and D. Liu, *J. Controlled Release*, 2012, **161**, 942–948.

 This journal is © The Royal Society of Chemistry 2018

Open Access Article. Published on 13 February 2018. Downloaded on 12/4/2025 9:16:04 PM.
This article is licensed under a Creative Commons Attribution-NonCommercial 3.0 Unported Licence.

23 R. M. Putri, J. J. L. M. Cornelissen and M. S. T. Koay, *ChemPhysChem*, 2015, **16**, 911–918.
24 L. Yang, A. Liu, S. Cao, R. M. Putri, P. Jonkheijm and J. J. L. M. Cornelissen, *Chem. – Eur. J.*, 2016, **22**, 15570–15582.
25 Z. Liu, J. Qiao, Z. Niu and Q. Wang, *Chem. Soc. Rev.*, 2012, **41**, 6178–6194.
26 M. G. Mateu, *Arch. Biochem. Biophys.*, 2013, **531**, 65–79.
27 A. Liu, C. H. H. Traulsen and J. J. L. M. Cornelissen, *ACS Catal.*, 2016, **6**, 3084–3091.
28 A. M. Wen and N. F. Steinmetz, *Chem. Soc. Rev.*, 2016, **45**, 4074–4126.
29 J. A. Luckanagul, K. Metavarayuth, S. Feng, P. Maneesaay, A. Y. Clark, X. Yang, A. J. García and Q. Wang, *ACS Biomater. Sci. Eng.*, 2016, **2**, 606–615.
30 P. Maturavongsadit, J. A. Luckanagul, K. Metavarayuth, X. Zhao, L. Chen, Y. Lin and Q. Wang, *Biomacromolecules*, 2016, **17**, 1930–1938.
31 J. A. Luckanagul, L. A. Lee, S. You, X. Yang and Q. Wang, *J. Biomed. Mater. Res., Part A*, 2015, 887–895.
32 J. Luckanagul, L. A. Lee, Q. L. Nguyen, P. Sitasuwan, X. Yang, T. Shazly and Q. Wang, *Biomacromolecules*, 2012, **13**, 3949–3958.
33 L. M. Bronstein, *Small*, 2011, **7**, 1609–1618.
34 C. A. Hommersom, B. Matt, A. van der Ham, J. J. L. M. Cornelissen and N. Katsonis, *Org. Biomol. Chem.*, 2014, **12**, 4065–4069.
35 C. W. Kuhn, *Phytopathology*, 1964, **54**, 853–857.
36 J. B. Bancroft, C. E. Bracker and G. W. Wagner, *Virology*, 1969, **38**, 324–335.
37 J. B. Bancroft, G. J. Hills and R. Markham, *Virology*, 1967, **31**, 354–379.
38 R. F. Garmann, M. Comas-Garcia, C. M. Knobler and W. M. Gelbart, *Acc. Chem. Res.*, 2016, **49**, 48–55.
39 M. Kwak, I. J. Minten, D. Anaya, A. J. Musser, M. Brasch, R. J. M. Nolte, K. Müllen, J. J. L. M. Cornelissen and A. Herrmann, *J. Am. Chem. Soc.*, 2010, **132**, 7834–7835.
40 J. Mikkilä, A. Eskelinen, E. H. Niemelä, V. Linko, M. J. Frilander, P. Törmä and M. A. Kostiainen, *Nano Lett.*, 2014, **14**, 2196–2200.
41 M. Comellas-Aragones, H. Engelkamp, V. I. Claessen, N. A. J. M. Sommerdijk, A. E. Rowan, P. C. M. Christianen, J. C. Maan, B. J. M. Verduin, J. J. L. M. Cornelissen and R. J. M. Nolte, *Nat. Nanotechnol.*, 2007, **2**, 635–639.
42 M. Comellas-Aragonès, A. de la Escosura, A. T. J. Dirks, A. van der Ham, A. Fusté-Cuñé, J. J. L. M. Cornelissen and R. J. M. Nolte, *Biomacromolecules*, 2009, **10**, 3141–3147.
43 M. Brasch, A. de la Escosura, Y. Ma, C. Uetrecht, A. J. R. Heck, T. Torres and J. J. L. M. Cornelissen, *J. Am. Chem. Soc.*, 2011, **133**, 6878–6881.
44 D. Luque, A. D. L. Escosura, J. Snijder, M. Brasch, R. J. Burnley, M. S. T. Koay, J. L. Carrascosa, G. J. L. Wuite, W. H. Roos, A. J. R. Heck, J. J. L. M. Cornelissen, T. Torres and J. R. Castón, *Chem. Sci.*, 2014, **5**, 575–581.
45 B. Dragnea, C. Chen, E. Kwak, B. Stein and C. C. Kao, *J. Am. Chem. Soc.*, 2003, **125**, 6374–6375.
46 C. Chen, M. Daniel, Z. T. Quinkert, M. De, B. Stein, V. D. Bowman, P. R. Chipman, V. M. Rotello, C. C. Kao and B. Dragnea, *Nano Lett.*, 2006, **6**, 611–615.
47 S. K. Dixit, N. L. Goicochea, M. Daniel, A. Murali, L. Bronstein, M. De, B. Stein, V. M. Rotello, C. C. Kao and B. Dragnea, *Nano Lett.*, 2006, **6**, 1993–1999.
48 X. Huang, L. M. Bronstein, J. Retrum, C. Dufort, I. Tsvetkova, S. Aniagyei, B. Stein, G. Stucky, B. McKenna, N. Remmes, D. Baxter, C. C. Kao and B. Dragnea, *Nano Lett.*, 2007, **7**, 2407–2416.
49 L. Yang, H. Yang, F. Li and X. Zhang, *Langmuir*, 2013, **29**, 12375–12379.
50 V. Hong, S. I. Presolski, C. Ma and M. G. Finn, *Angew. Chem., Int. Ed.*, 2009, **48**, 9879–9883.
51 J. D. Miller, E. D. Baron, H. Scull, A. Hsia, J. C. Berlin, T. McCormick, V. Colussi, M. E. Kenney, K. D. Cooper and N. L. Oleinick, *Toxicol. Appl. Pharmacol.*, 2007, **224**, 290–299.
52 S. Makhseed, M. Machacek, W. Alfadly, A. Tuhl, M. Vinodh, T. Simunek, V. Novakova, P. Kubat, E. Rudolf and P. Zimcik, *Chem. Commun.*, 2013, **49**, 11149–11151.
53 L. B. Josefsen and R. W. Boyle, *Theranostics*, 2012, **2**, 916–966.
54 S. Li, H. Cheng, B. Xie, W. Qiu, J. Zeng, C. Li, S. Wan, L. Zhang, W. Liu and X. Zhang, *ACS Nano*, 2017, **11**, 7006–7018.
55 E. Cavatorta, M. L. Verheijden, W. van Roosmalen, J. Voskuhl, J. Huskens and P. Jonkheijm, *Chem. Commun.*, 2016, **52**, 7146–7149.
56 S. Sankaran, M. C. Kiren and P. Jonkheijm, *ACS Nano*, 2015, **9**, 3579–3586.
57 J. Song, X. Yang, O. Jacobson, L. Lin, P. Huang, G. Niu, Q. Ma and X. Chen, *ACS Nano*, 2015, **9**, 9199–9209.